All-plastic miniature fluorescence microscope for point-of-care readout of bead-based bioassays

Alessandra Forcucci
Michal Emanuel Pawlowski
Zachary Crannell
Ina Pavlova
Rebecca Richards-Kortum
Tomasz S. Tkaczyk

SPIE.

All-plastic miniature fluorescence microscope for point-of-care readout of bead-based bioassays

Alessandra Forcucci, Michal Emanuel Pawlowski, Zachary Crannell, Ina Pavlova, Rebecca Richards-Kortum, and Tomasz S. Tkaczyk*
Rice University, Department of Bioengineering, 6100 Main Street, Houston, Texas 77005, United States

Abstract. A number of new platforms have been developed for multiplexed bioassays that rely on imaging targeted fluorescent beads labeled with different fluorescent dyes. We developed a compact, low-cost three-dimensional printed fluorescence microscope that can be used as a detector for mutiplexed, bead-based assays to support point-of-care applications. Images obtained with the microscope were analyzed to differentiate multiple analytes in a single sample with a comparable limit of detection to commercially available macroscopic assay platforms. © *2015 Society of Photo-Optical Instrumentation Engineers (SPIE)* [DOI: 10.1117/1.JBO.20.10.105010]

1 Introduction

The World Health Organization has called for an increase in access to reliable diagnostic tests in low-resource areas.[1] Access to diagnostic devices is integral to reducing long-term complications that may result from diseases, such as HIV/AIDS, malaria, respiratory infections, perinatal conditions, and diarrheal diseases.[2] Point-of-care (POC) tests often require an optical system for signal detection as well as imaging, and in low-resource environments, size, cost, and infrastructure requirements of these optical systems are critical.[3]

POC diagnostics that do not require operation by highly trained laboratory staff are used to rapidly provide results to patients at a lower cost than conventional laboratory analysis would entail. These diagnostic devices may eliminate the need for samples to be sent to a lab for analysis. These POC devices are typically designed for targets such as proteins, metabolites, and other small molecules, nucleic acids, human cells, and microbes or pathogens. Fluorescence signal detection is a commonly used technique to detect and diagnose infectious and hematological diseases due to its high sensitivity and specificity, and bench-top detection systems, especially those that perform fluorescence signal detection, often require expensive illumination sources and multiple optical elements, such as lenses and emission and excitation filters.

To reduce instrumentation costs that are typical for commercial fluorescence microscopy systems, several groups have used three-dimensional (3-D) printing to develop custom optical instrumentation. The CellScope, a 3-D printed microscope designed to attach to a cellular phone, developed by the Fletcher group, is an example of one portable device that uses commercially available optics. It consists of a commercially available objective [0.85 numerical aperture (NA), 60× Achromat] and a commercially available 20× wide-field eyepiece, resulting in a system field of view (FOV) of 180 μm in diameter, a magnification of 28×, and a resolution of 1.2 μm.[4] The CellScope

Oto, a digital otoscope sold commercially by the group, currently retails for $299 USD.[5] The CellScope Oto is designed to perform ear exams at the POC via digital brightfield imaging. The device does not operate in fluorescence mode; therefore, the listed price does not include components found in these typically more expensive systems, such as excitation and emission filters. The price also does not take into account the cost of the detector (iPhone). When compared to scientific cameras, cell phone cameras restrict the adjustment of capture parameters, such as exposure time, master gain, and relative color gain.[6] Additionally, with a mobile phone camera, users are unable to set processing parameters, such as compression, custom corrections, edge enhancement, and noise reduction.[6] Although the user interface is simplified through use of a mobile phone camera, control of image capture and processing is sacrificed.

The Ozcan group also created a cost-effective microscope cell-phone attachment.[7] This attachment combines commercially available optics and 3-D printed optomechanics to create a transmission microscope that interfaces with a modified flow cytometer to quantify white blood cells in blood samples and can resolve features on the order of 2 to 4 μm.[7] This attachment is low cost (estimated at <10 USD in mass production) but can only perform tests using two LEDs of the same color. Also, the plastic filter used is an absorption filter, which reduces the overall device cost but does not permit narrowband excitation of a sample.

Other 3-D printed microscopes designed for global health applications, such as the Global Focus Microscope, use low-cost components such as LED flashlights containing a white LED for brightfield imaging and a blue LED with narrow band excitation filter for fluorescence. The Global Focus Microscope is designed specifically for a single application, fluorescence, and brightfield imaging of *Mycobacterium tuberculosis* samples.[8] The Global Focus Microscope uses multiple commercially available microscope objectives for brightfield and fluorescence imaging, however, it is limited in the versatility of its fluorescence applications since the filters and illumination source are

---

*Address all correspondence to: Tomasz S. Tkaczyk, E-mail: ttkaczyk@rice.edu

specifically chosen for auramine orange fluorescent dye. The estimated cost of the prototype was $240 USD.

Many portable fluorescence systems designed for the POC, including the CellScope and Global Focus Microscope, use high-power LEDs as light sources due to their long lifetime (∼50,000 h), ambient operating temperature, and low power requirements in addition to their low cost.[9] Traditional fluorescence microscopy illumination setups typically use high-energy, expensive light sources such as xenon or mercury arc lamps. These bulky illumination sources are unsuitable for work in the field since the bulbs are delicate and provide illumination for only ∼200 h.[10] Our prototype device uses two high-power LEDs to provide dual excitation for multiplexed imaging. Instrumentation costs will typically increase if quantification of signal in samples with multiple fluorescence emission channels is needed to make more informed diagnoses at the POC setting. The Ligler group has developed a microflow cytometer platform for performing multiplexed bead-based assays. Multiplexed microsphere immunoassays using the system were successfully performed for six discrete bacteria and toxins and the microflow cytometer produced results comparable to that of commercial systems.[11] Recently, this group fabricated a spinning magnetic trap platform. This platform, the MagTrap, interfaces with magnetic core polystyrene microbeads.[12] The MagTrap system was integrated with the existing microflow cytometer to automate sample preparation and detect multiple pathogens simultaneously.[12]

There has also been ongoing development of bench-top readers with high specificity and sensitivity, which have the potential to screen for a large number of targets simultaneously.[13,14] Currently, a number of such bench-top instruments for molecular assays are available on the market.[15,16] Luminex's MAGPLEX system of labeled beads is one such technology that exemplifies spatial multiplexing. The MAGPIX fluorescent detection system utilizes magnetic MagPlex microspheres and Luminex's XMAP technology to measure multiple proteins or nucleic acids in a single reaction.[17] The Luminex system utilizes preset ratios of two dyes dissolved in their polymer beads, which exhibit peak emission at two discrete wavelengths.[18] The antibody or capture oligomer for a given target is immobilized on beads with a particular dye ratio, and readout in a cytometry-like fashion includes identifying the bead type according to the ratio of the two dyes (excited by a common wavelength) and quantifying the bound target using a different excitation wavelength for a fluorescent label.[19] The beads are illuminated by two LEDs and multicolor fluorescence images are analyzed to classify the analyte being detected and to determine its concentration.[20] Although the system reduces the cost of traditional assays and reduces the required sample volume, the MAGPIX reader is not suited for POC applications. It is bulky and expensive, measuring $16.5 \times 60 \times 43 \text{ cm}^3$ with a weight of 38.5 pounds and retail cost of ∼35,000 USD.[21]

The sections that follow describe a low-cost prototype of a miniature optical detection system designed for POC optical readout of bead-based bioassays. The system was fabricated using the rapid prototyping techniques of diamond turning and high-resolution 3-D printing. The system is modular and contains two main subunits: a miniature microscope and an illumination system designed for two fluorescent excitation pathways. Single-point diamond turning was used to fabricate all custom lenses in the prototype miniature system. Single-point diamond turning is primarily used to fabricate inserts for lenses

for injection molding and has been well documented as a method by which to fabricate high performance, custom miniature plastic lenses.[22–26]

Unlike the low-cost prototypes discussed previously,[3–8] our modular prototype can independently excite two fluorophores. It may be used in brightfield or fluorescence modes and has three fluorescent emission channels. Unlike many other low-cost microscopes,[5,7] our prototype was designed with a specific application in mind (multiplexed bead-based bioassays). The illumination system contains two high-power LEDs to provide dual excitation for multiplexed imaging. The initial sample for demonstrating successful optical readout was the MagPlex bead platform due to its commercial availability and simple sample preparation, though the modular nature of the assembled prototype provides versatility for future applications. The stackable, modular optomechanics units were made via 3-D printing, an additive rapid fabrication process that is used to make components of custom geometries and sizes, such as the tunable objective lens holder and tube lens holder used in the miniature microscope subunit. Unlike the Cellscope and other cell-phone based platforms,[4–7] our device uses a low-cost board-level camera. The use of a board-level camera ensures that the user can, if necessary, modify image acquisition settings, which is difficult or impossible to do on many cellular phones. The diffraction-limited optical design is monochromatic, which relaxes manufacturing tolerances and simplifies overall design and assembly. Single-point diamond turning of prototype plastic lenses is used to create the custom spherical and aspheric lenses. The all-plastic composition of the prototype, including the diamond-turned poly(methy methacrylate) (PMMA) objective and tube lenses, is critical for demonstrating the potential for the device to be mass produced via injection molding. Our resulting POC prototype is 1.5 orders of magnitude cheaper than its commercially available counterpart, Luminex's MAGPIX, and can perform comparable analyte classification and quantification.

2 Experimental Methods

For the prototype system, optical readout of bead-based bioassays was validated using Luminex's system of MagPlex beads due to their simple experimental preparation and commercial availability. The spectral properties of the MagPlex beads are described in Sec. 2.1. Sections 2.2 and 2.3 describe the optical design of the miniature microscope and illumination system, respectively. Sections 2.4.1 and 2.4.2 describe the design and fabrication process for the microscope and illumination optomechanics, respectively.

2.1 Luminex's MagPlex Beads

The MagPlex microspheres are magnetic core-containing polystyrene beads that are 6.5 μm in diameter.[12] There are two fluorophores present in the MagPlex beads, referred to as classifier 1 (CL1) and classifier 2 (CL2), which allow the beads to be identified by an optical reader. The classifier 1 dye has excitation and emission peaks at 615 and 661 nm, respectively, and clad the classifier 2 dye has excitation and emission peaks at 615 and 720 nm, respectively. When irradiated by a common excitation channel, the bead type can be identified by the ratio of the intensity of the two classifier dyes. Each bead type is functionalized with a different type of oligonucleotide capture sequence complementary to a target sequence of interest. Extended polymerase chain reaction products are biotinylated, hybridized to the beads, and labeled with a streptavidin coupled "reporter"
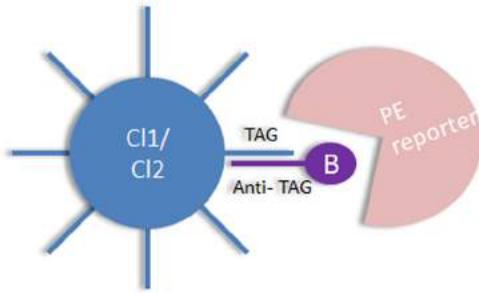
Fig. 1 This figure illustrates the MagPlex bead hybridization. B is biotin and PE is streptavidin phycoerythrin. The classifier (CL1/CL2) channels determine the analyte being detected while the magnitude of the PE-derived signal is measured in the reporter channel.

Table 1 Summary of optical parameters of miniature fluorescent microscope.

NA image side	0.25
Magnification	−4×
Telecentric object space	Yes
Object side field of view diameter	1.2 (mm)
Objective working distance	1.2 (mm)
Design wavelength	590 (nm)
Largest clear aperture (first surface of the tube lens)	8.07 (mm)
"Infinity space" length	15 (mm)
Total length of optical system	43.02 (mm)

fluorescent dye (Fig. 1). The reporter dye has an excitation peak at 510 nm and an emission peak at 590 nm.

2.2 Optical Design of Miniature Fluorescence Microscope

An optical schematic of the miniature fluorescence microscope that was designed for the preliminary application of the optical readout of bead-based bioassays is presented in Fig. 2.

The microscope objective and tube lens were custom designed using Zemax® (Radiant Zemax, Redmont, Washington). A summary of the basic optical parameters of the microscope is presented in Table 1. Note that the optical system presented in Fig. 2 has flat object and image surfaces.

The optical prescription data of the microscope objective and the tube lens are given in Table 2. The microscope objective has an NA of 0.25, focal length of 4 mm, and a 1.2-mm diameter FOV. The tube lens has a focal length of 16 mm, and together with the objective, forms an infinity-corrected microscope.

The microscope objective and tube lens were designed to be infinity corrected to increase system flexibility. This flexibility enables switching of components auxiliary to the imaging system, such as filters, prisms, and polarizers, without affecting the image-object plane location and resolution. The combined magnification of the microscope is −4×. The microscope objective is built from three aspheric lenses, is 11.34-mm long, and has a maximum clear aperture diameter of 4 mm. The tube lens, due to the "infinity space" length of 15 mm, has the largest clear aperture, measuring 8 mm. The tube lens is 7.5-mm long and consists of two elements, one spherical and one aspheric. The total length of the optical system is 43 mm, which is a length comparable to many commercial microscope objectives.

For example, the Zeiss Primo Plan-Achromat 10 × /0.25 is 40-mm long, as measured from front lens to stop face.

To simplify the optical design and relax the manufacturing tolerances, the system was optimized for a single wavelength. The objective and the tube lens are made exclusively from PMMA due to its excellent machinability on diamond turning machines[27,28] and low autofluorescence.[24] The modulation transfer function (MTF) that was calculated using the fast Fourier algorithm for the design wavelength in nominal working conditions is presented in Fig. 3(a), together with the corresponding spot diagram plot depicted in Fig. 3(b).

The design was optimized for eight field points, evenly distributed along the Y-field object axis from 0 to 0.6 mm. The MTF and the spot diagram plots shown in Fig. 3 indicate diffraction-limited performance for all field points for nominal working conditions. The small deviation of the sagittal MTF plot for a marginal field point indicates the presence of uncorrected astigmatism, but at a level that is not detrimental to overall system performance. Diffraction-limited performance of the miniature fluorescence microscope was achieved due to extensive use of aspheric components throughout the design.

The optical system of the microscope was designed in a two-stage process. In stage one, the microscope objective was designed, and in stage two, the tube lens was designed. We corrected aberrations of the microscope objective and the tube lens individually, i.e., aberrations of the microscope objective were not corrected by the tube lens and vice versa. This complicated
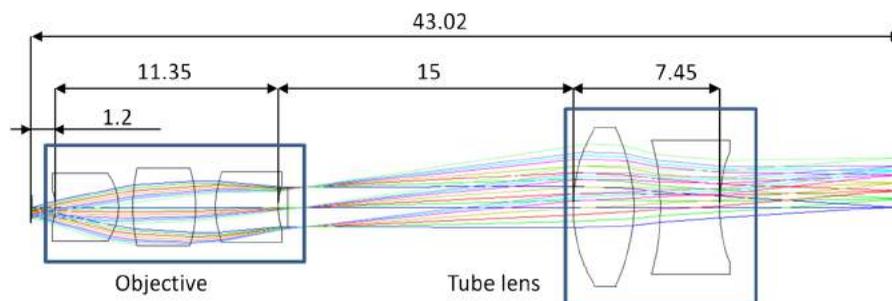
Fig. 2 The optical schematic of the miniature fluorescence microscope. All dimensions given are in millimeters (mm).

Table 2 Optical prescription data of miniature fluorescent microscope.

| Surface	Radii	Thickness	Glass	Semidiameter	Conic
0	∞	1.200		0.600	
1	−2.565	3.125	PMMA	0.868	1.839
2	−3.032	0.732		1.738	0.062
3	9.389	3.200	PMMA	1.930	−2.937
4	−7.061	1.001		1.981	−0.746
5	4.749	3.200	PMMA	1.793	0.194
6	3.817	0.500		1.152	0.955
7	∞	14.500		1.014	
8	7.380	3.108	PMMA	4.035	−0.954
9	−7.859	1.345		3.962	−2.875
10	−12.868	3.000	PMMA	3.403	
11	7.775	9.215		2.793	
12	∞			2.501	

Note: Radii, thicknesses, and semidiameters are in units of millimeters(mm). PMMA, poly(methy methacrylate).

the design but resulted in compatibility of the microscope objective and tube lens with a large selection of commercially available infinity-corrected systems. The expected system performance was evaluated using the root mean square (RMS) wavefront error during the design process. The RMS wavefront error of the microscope optical train was 0.054 for nominal working conditions. The fabrication tolerance parameters used during the optimization stage are presented in Table 3.

Based on 10,000 runs of Monte-Carlo simulations, it was estimated that the miniature fluorescence microscope would achieve diffraction-limited performance on axis with an 80% probability and there would be a 20% of chance of reaching diffraction-limited performance within the FOV enclosed by a disk of radius of 0.42 mm (70% of object height). The estimated change in performance due to manufacturing tolerances calculated using the root sum square algorithm was estimated to be 0.058 and the total estimated system performance (nominal + change) was estimated to be 0.112. In nominal working conditions, as defined by the Rayleigh criteria, diffraction effects will limit the resolution of the miniature fluorescent microscope to ∼1.4 μm. Taking the size of the target objects (6.5 μm) and the system resolution into account, we accepted the predicted performance of the system because our application did not require a diffraction-limited 0.25 NA imaging system for sufficient object sampling.

The tube lens and microscope objective were manufactured on the Precitech Optimum 2400 (Ametek, Precitech, Keene, New Hampshire) diamond turning lathe. Pellets of optical grade plastics were mounted on the diamond turning machine using ER16-UP (Rego-Fix, Tenniken, Switzerland) collets housed in a custom vacuum chuck compatible holder. ER16-UP collets limited the diameter of manufactured parts to 10 mm, which was taken into account during the design stage. Diamond turning paths were generated using the diamond turning path generator (DTPG v2.54, Precitech) program based on the Zemax lens drawings. In order to simplify assembly of the system, lenses were manufactured with integrated spacing features and were stacked inside brass hypodermic tubes. The outer diameter (OD) of all lenses was manufactured to meet tight, interference fit tolerances with the inner diameter of brass tubes. Both brass tubes
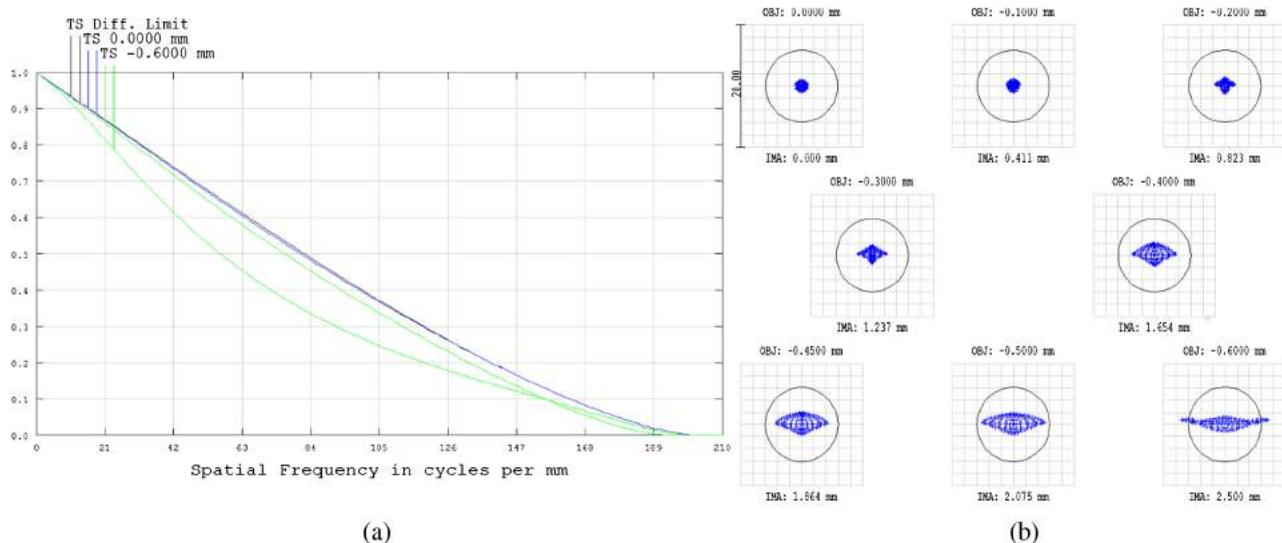
Fig. 3 Performance metrics of the miniature tunable fluorescence microscope for nominal working conditions: (a) modulation transfer function (MTF) plots for two tangential field points located on optical axis and −0.6 mm away from it. MTF plots for tangential and sagittal field points are drawn in blue and for field point located −0.6 mm away from the optical axis in green. Tangential and sagittal MTF plots for diffraction limited system are drawn in black. All MTF plots are for the design wavelength of 590 nm. (b) Spot diagrams for all designed, tangential field points of: 0.0 mm, −0.1 mm, −0.2 mm, −0.3 mm, −0.4 mm, −0.45 mm, −0.5 mm, −0.6 mm, for design wavelength of 590 nm. Horizontal extent and vertical extent of subfield rectangles: 20 nm. The airy disk is depicted in spot-diagram subfield images as a black circle. The theoretically calculated airy disk radius is 5.9 μm.

Table 3 Tolerance parameters of the miniature fluorescent microscope.

Parameter	Radii (%)	Thickness (mm)	Element decenter (mm)	Element tilt (deg)	Surface decenter tilt (mm)	Irregularity (fringes)	Abbe (%)	n (a.u.)
Value	0.4%	0.035	0.02	0.03	0.02	0.2	0.574	0.001
		0.2[a]						

[a]For surface 7 (infinity space).

that held the microscope and tube lens assemblies had an ~1-mm wide slit cut throughout their lengths parallel to the mechanical axis of the optical system, which allowed noninvasive insertion of the fragile plastic lenses. Elastic expansion of the brass tubes, due to interference fit between the lenses' OD and tube internal diameter (ID), resulted in a radial clamping force, with its vector pointing toward the mechanical axis of the optical system that held both the microscope objective and tube lens assemblies.

The microscope objective was mounted inside a hypodermic brass tube that had a 7.13 mm OD and a 6.34-mm ID. The tube lens assembly was inserted into a brass tube with a 10.32-mm OD and a 9.54-mm ID. A drawing of the optical system assembly of the microscope objective is presented in Fig. 4(a). A schematic of the optomechanical assembly of the tube lens is depicted in Fig. 4(b).

The assembled prototypes of the microscope objective and tube lens were tested individually on the Zeiss Axio Imager Z1 (Zeiss, Oberkochen, Germany) microscope. We limited stray light via internal blackening of the brass hypodermic tubes and coating of lens spacing stop surfaces with permanent marker prior to inserting the lenses. Additionally, before testing, we masked nonactive front and back areas of both systems (tube lens and microscope objective) with laser cut stops, made from thin, volume blackened plastic. The prototypes were mounted sequentially in a custom designed 3-D printed holder, which interfaced with the Zeiss microscope's revolving nosepiece. The resolution of the system components was assessed using positive, high-resolution 1951 USAF resolution test (Stock No.: 58-198, Edmund Optics, New Jersey). The Zeiss standard halogen illumination unit was used with a narrowband, 656-nm

filter with a 10-nm bandwidth (#65-656, Edmund Optics) inserted in the illumination path. We tested all components of the system at a wavelength of 656 nm to use the 1951 USAF target for quality assessment, since at the design wavelength of 590 nm, the lens will out-resolve the high-resolution 1951 USAF target, making testing with a commercially available resolution target impossible. Images of the 1951 USAF resolution target were acquired through a standard 1× microscope tube lens using a black and white Axiocam MRm camera (Zeiss).

Three optical systems were tested to individually assess the optical performance of each: the miniature plastic microscope objective, the miniature plastic tube lens, and a commercially available Zeiss 10 × /0.25 objective. Raw images of the resolution target recorded using the miniature fluorescent microscope objective, the miniature tube lens, and the Zeiss objective are presented in Figs. 5(a)–5(c), respectively.

The miniature microscope objective was tested in nominal, designed working conditions, with the resolution target located in the object plane. The tube lens was tested in reverse, with 1951 USAF resolution target located in its designed image plane. The Zeiss microscope objective was tested in nominal working conditions to provide a reference point for the components of the miniature system. All three tested lenses have different focal lengths, which in the infinity-corrected set-up of the Zeiss microscope resulted in different magnifications of the 1951 USAF target images.

The spatial resolution of the microscope objective was measured to be $\nu_{\mathrm{ob\,at\,656\,nm}} = 575$ lp/mm. The spatial resolution of the tube lens was measured to be $\nu_{\mathrm{tb\,at\,656\,nm}} = 203$ lp/mm. The Zeiss microscope objective successfully resolved features up to $\nu_{\mathrm{zeiss\,at\,656\,nm}} = 287$ lp/mm. Theoretically, a diffraction-limited
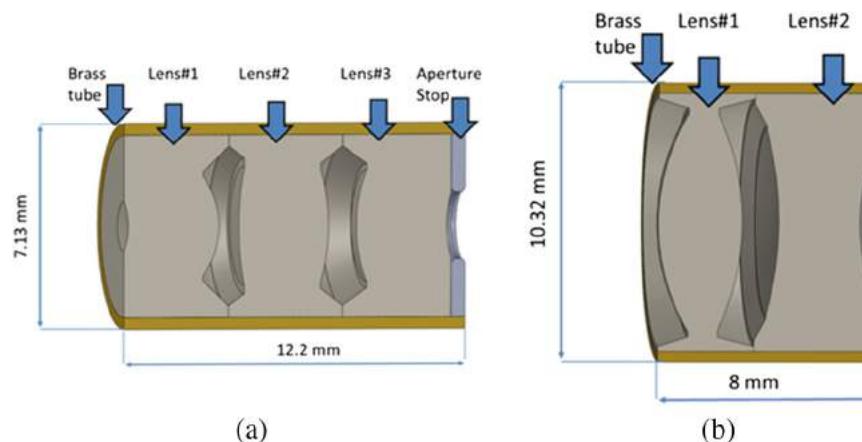
Fig. 4 Cross-section through three-dimensional model of the optomechanical assembly of the (a) microscope objective and (b) the tube lens.
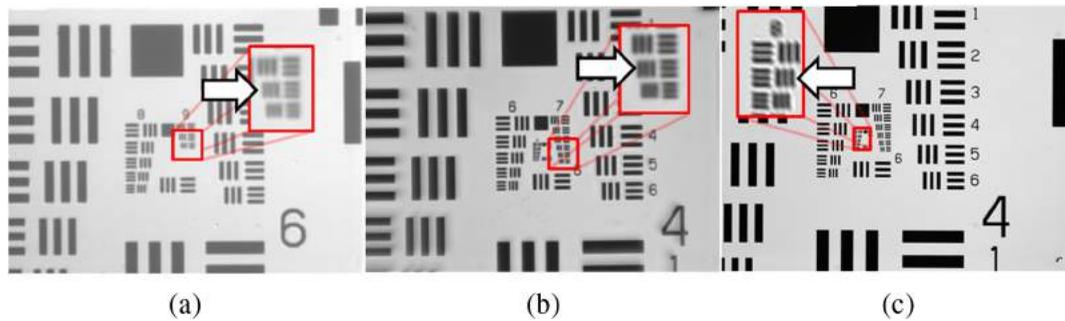
Fig. 5 Images of 1951 USAF resolution target taken using Zeiss Axio Imager Z1 through: (a) miniature all plastic microscope objective, (b) miniature plastic tube lens, and (c) reference Zeiss $10 \times /0.25$ microscope objective. Please note that due to difference in focal lengths of tested systems, images of resolution target were recorded at different magnifications. Magnified, red marked regions of 1951 USAF resolution target, close to assessed limit of resolution are zoomed and presented in inlays in respective images.

0.25 NA objective at a wavelength of 656 nm, according to Rayleigh criterion, should resolve $\nu_{\text{theo at 656 nm}} = 625$ lp/mm, a spatial resolution located in group 9 between elements 2 and 3. Our microscope objective successfully resolved both horizontal and vertical features of element 2 group 9 as well as horizontal features of group 9 element 3, confirming a satisfactory, as designed, diffraction-limited performance. The tube lens in nominal "as designed" working conditions has an image NA of 0.063 and theoretically, according to Rayleigh criterion, when illuminated with wavelength of 656 nm should resolve spatial features up to $\nu_{\text{RTL}} = 157$ lp/mm (a spatial frequency located in group 7 between elements 2 and 3). Because the tube lens was designed independently from the objective so that it may interface with the future generation custom-designed miniature infinity-corrected objectives of higher NAs (e.g. NA of 0.5), it has a clear aperture larger than that required to interface with the 0.25 NA objective lens). The tube lens was tested with the microscope Koehler illumination aperture set to an NA of 0.1 (the minimum NA of the illumination possible on the Zeiss system). The system was designed to work with an illumination beam of 0.063 NA, but for experimental settings using an illumination NA of 0.1, the expected spatial resolution limit was met (203 lp/mm). Because the tube lens was designed independently from the objective so that it may interface with future generation custom-designed miniature infinity-corrected objectives of higher NAs (e.g., NA of 0.5), it has a clear aperture larger than that required to interface with the 0.25 NA objective lens. Due to the higher than designed illumination beam NA, we were able to resolve 203 lp/mm features on the 1951 USAF target, but at the cost of an unwanted increase of stray light (clearly visible on the edges of the image of the 1951 USAF target).

The miniature microscope objective as directly compared to commercially available 0.25 NA objectives exhibited higher resolution but visibly lower contrast. While our system out-resolved the commercial microscope objective, it should be noted that we compared the performance of both systems for a single wavelength. Resolution of commercially available achromatic microscope objectives is a result of balance between spectral range, optomechanical complexity, and cost. We attribute decreased contrast of the miniature microscope objective and tube lens compared to the reference commercial objective to stray light leaking through them.

## 2.3 Optical Design of Illumination System

The optical schematic for the illumination system is shown in Fig. 6.

The dual wavelength Abbe illumination system, shown in Fig. 6, was designed using Zemax®(Radiant Zemax) based on the peak excitation wavelengths of the MagPlex microspheres described in Sec. 2.1. Abbe illumination is characterized by imaging the source directly onto the sample plane.[29] This illumination configuration was designed primarily to reduce the number of optical elements (e.g., lenses). Spectral characteristics of filters and light sources used in the classifier channels are presented in Fig. 7(a). The excitation filter, emission filter, and LED spectra for the reporter channel are shown in Fig. 7(b).

The reporter illumination pathway, highlighted in blue in Fig. 7, consists of a 505-nm LED (part no. SR-01-E0070, Luxeon), a commercially available collector lens (ACL1210, Thorlabs), a bandpass filter (FF03-510/20, Semrock), two long-pass filters to block UV light from exciting the polystyrene substrate of the MagPlex beads (BLP01-355R and BLP01-442R,
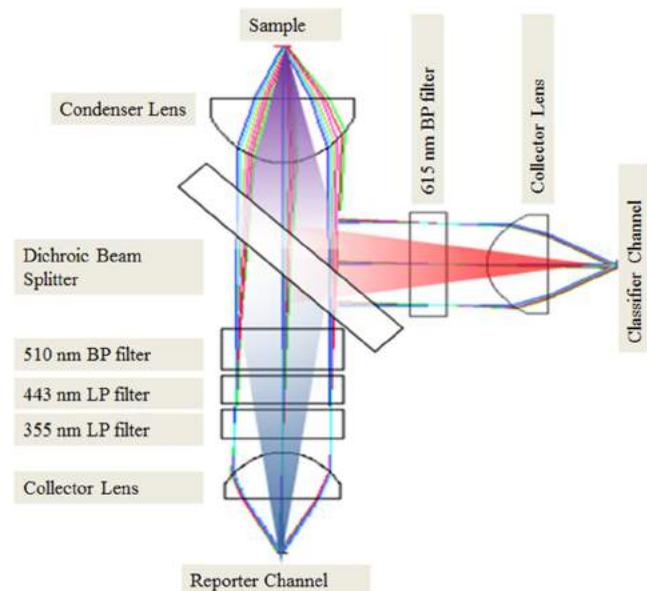
Fig. 6 Optical layout of the dual wavelength illumination system.

(a)

(b)
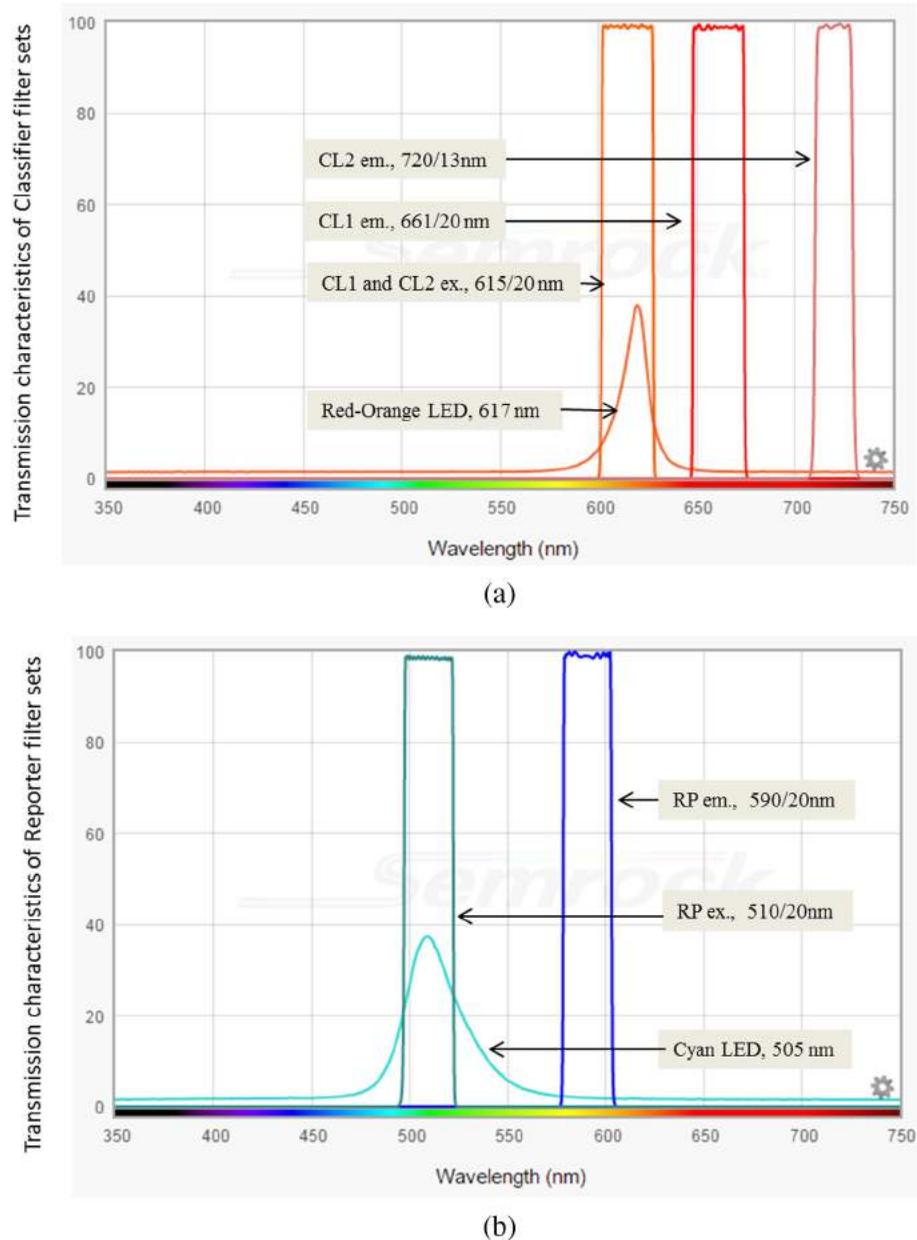
Fig. 7 Spectral bandwidths of excitation (ex.) and emission (em.) filters together with spectral densities of illumination sources for (a) classifier and (b) reporter channels.

Semrock), and a dichroic mirror (DMLP567, Thorlabs). A second commercially available aspheric was used as the condenser lens for both the classifier and reporter channels (ACL1512, Thorlabs).

The classifier excitation optical path, highlighted in red in Fig. 7, has an analogous layout to the reporter pathway. The pathway elements include a 617-nm LED (part no. SR-01-H2060, Luxeon), a commercially available aspheric collector lens (ACL1215, Thorlabs, USA) and a bandpass filter centered at 615 nm (FF01-615/20, Semrock). The classifier illumination pathway shares the dichroic mirror and condenser lens common to the reporter pathway. The common pathway for the two channels is shown in purple in Fig. 6.

Uniformity of illumination is contingent on proper alignment of all optical elements. Elements in the illumination channels (lenses, filters, etc.) are press-fit into 3-D printed housing.

The ProJet HD 3000 3-D printer has an accuracy on the order of 0.025 to 0.05 mm/in. of the part dimension, which may cause slight element misalignment. The lenses are positioned in 3-D printed indented holders and are held in place via printed alignment features once the two mirrored halves of the illumination housing are pressed together. The LED and heat sink are mounted in a 3-D printed slot that holds them centered on the optical axis of each illumination pathway. The 3-D printed hardware of the illumination system eliminates the need for expensive commercial optomechanics and allows for rapid iterative prototyping and rebuilding. A potential downside to 3-D printed alignment features is that printer tolerances and plastic shrinkage may compromise alignment of optical elements.

In the classifier and reporter pathways, the illumination field uniformity varied between 11% and 13%, respectively. Experimental validation on multiple images, however, showed
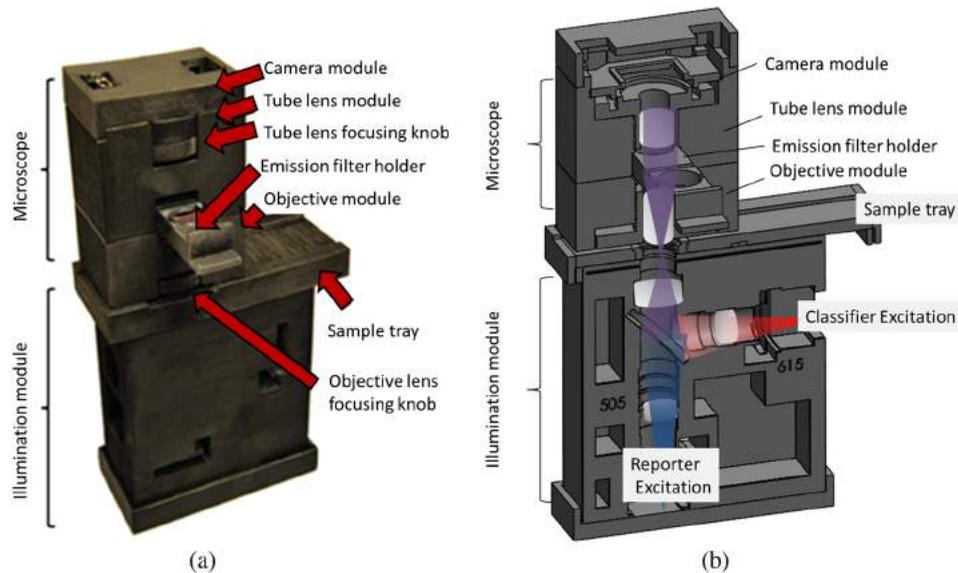
Fig. 8 (a) A photo of the complete miniature system prototype. The system contains (from top to bottom) a camera, a tube lens, a sliding emission filter holder, an objective lens, a sample tray that is designed to fit a standard size microscope slide, and an illumination module that houses optics and light sources for two different illumination pathways. (b) A Solidworks rendering of the cross-section of the complete system. A cross-section of the camera mount, adjustable tube and objective lens holders, emission filter holder, sample tray, and illumination module is shown. In the illumination module, the classifier channel pathway is highlighted in red and the reporter channel illumination pathway is highlighted in blue. Both channels intersect at a dichroic beamsplitter and then share a subsequent common optical pathway, highlighted in purple.

that the intensity differences between all observable beads in the three channels were high enough to allow for accurate classification, indicating that these background intensity fluctuations have little influence over system performance. In addition, geometric properties such as bead size are measured to eliminate beads that are barely visible in the sample.

2.4 Optomechanical System

All optomechanical components of the miniature system were designed in Solidworks (Solidworks Premium, Dassault Systèmes SolidWorks Corporation) and fabricated on a 3-D printer (ProJet HD 3000, 3-D Systems). After printing, all system components were airbrushed matte black with enamel paint (Matte Black 33 A0360, Humbrol, United Kingdom) over internal and external surfaces. Additional light-blocking masks were laser cut from thin sheets of volume blackened plastic and placed under the sample tray as well as between the objective and tube lens holders. A labeled photograph and Solidworks design of the complete modular miniature system are shown in Figs. 8(a) and 8(b), respectively.

2.4.1 Miniature microscope optomechanics

A Solidworks rendering of the miniature infinity-corrected microscope is shown in Fig. 9.

The miniature infinity-corrected microscope sits above the sample tray, which was designed to hold a standard microscope slide. The objective lens is enclosed in a threaded holder, shown in Fig. 9, which allows for manual focus adjustment using a focusing knob. The ProJet HD 3000 3-D printer has a lateral resolution of 13×13 dots/mm in x and y. The axial resolution is 24 dots/mm with accuracy of 0.025 to 0.05 mm/in.,

depending on the part geometry. The high lateral resolution ensures that the tube lens and objective lens may be aligned on-axis in the 3-D printed housing without the need for additional machining or alignment features, since the lateral printer resolution falls within the design tolerances values listed in Table 3. The high axial resolution of the printer allows for printing of fine mechanical features, such as the 0.0635 millimeter pitch threading on the objective and tube lens holders, which enable fine manual adjustments of the objective and tube lens. The theoretical depth of field of the 0.25 NA objective lens corresponds to $\text{DoF} = (\lambda/2\text{NA}^2) = 4.72 \ \mu\text{m}$ at the design wavelength of 590 nm. The monochromatic objective lens requires a focal adjustment of 30 μm between the fluorescent channels, corresponding to a half rotation of the objective
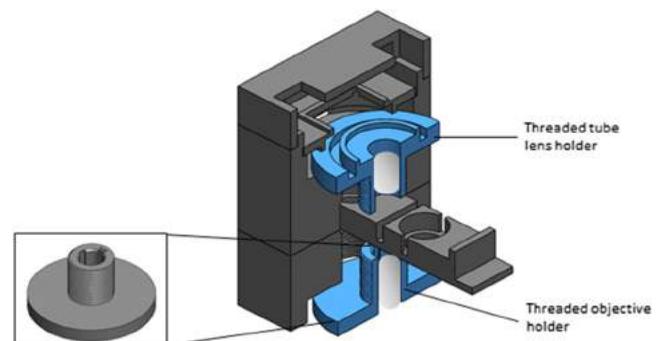
Fig. 9 A cross-section of a Solidworks rendering of the miniature microscope is shown above. The rendering illustrates an exploded view of the system cross section highlighting the threaded objective and tube lens holders. The inset image shows an enlarged view of the threaded objective holder.
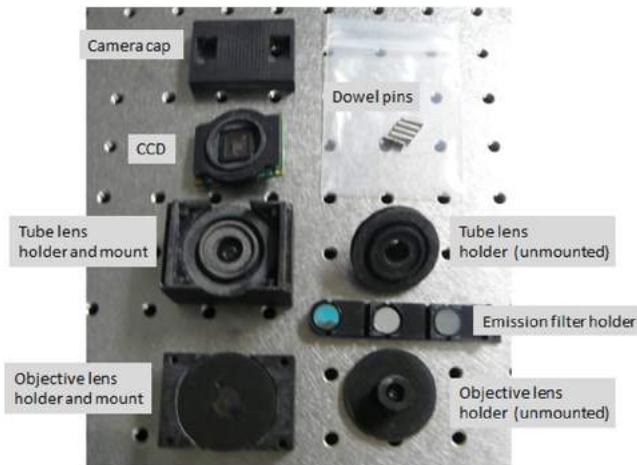
Fig. 10 The disassembled infinity-corrected miniature microscope components (camera cap, camera mount, objective mount, tube lens mount, and emission filter holder). Examples of the 3/10 dowel pins (Brikksen, Germany) used to connect the modules are shown in the top right corner. Dowel pin holes are visible on the tube and objective lens modules. Extra unmounted tube lens and objective lens modules are shown to the right of the microscope.

holder. The large depth of focus of the tube lens does not require manual adjustment between classifier and reporter emission channels.

The removable emission filter holder is inserted into the infinity-space above the microscope objective lens and below the tube lens. It houses three emission filters; one for each classifier channel and one for the reporter channel. Classifier channel 1 uses a bandpass emission filter centered at 661 nm (FF01-661/20, Semrock), classifier channel 2 uses a bandpass emission filter centered at 720 nm (FF01-720/13 nm, Semrock), and the reporter channel uses a bandpass emission filter centered at 590 nm (FF01-590/20, Semrock). All filters were ordered in custom 1/2-in. diameter housing to fit the small footprint of the microscope.

To reduce costs, we used an inexpensive CCD, the Pointgrey Chameleon CCD Monochrome Camera (CMLN-13S2M-CS, Point Grey Research Inc, Canada). The camera was dismounted to board level and placed in the custom 3-D printed camera mount above the tube lens holder. The camera was connected to a laptop via USB 2.0 cable for image acquisition and transfer. A photograph of the disassembled miniature microscope modules is shown in Fig. 10. Note that dowel pins were used to connect the modules.

2.4.2 Illumination optomechanics

The dual wavelength Abbe illumination module delivers light to a sample chamber designed to fit a standard microscope slide. The slide is inserted through a slot and can be manually adjusted to acquire images in multiple fields of view. A photograph view of the illumination unit cross-section and its components are shown in Fig. 11. Note that unlike the miniature microscope components, the components of the illumination system (heat sinks, Peltier coolers, LEDs, lenses, filters, and dichroic beamsplitter) are aligned via press fitting, rather than stacked and aligned with dowel pins in standalone modules.

2.5 Sample Preparation

For experiments with data collected using the miniature microscope, DNA hybridization to MagPlex-TAG microsphere beads (MTAG-XXX, Luminex) was performed according to the manufacturer's instructions with the following modifications: the beads were diluted and filtered through a 3.0-μm filter and resuspended in hybridization buffer prior to hybridization. Biotinylated DNA oligonucleotides complimentary to bead numbers 39 (5′-biotin-ACAAATATCTAACTACTATCACAA-3′), 73 (5′-biotin-CTTTATCAAATTCTAATTCTCAAC-3′), and 78 (5′-biotin-TTTACAAATCTAATCACACTATAC-3′) were purchased from IDT (USA). For each hybridization experiment, a dilution series was prepared for each bead such that there
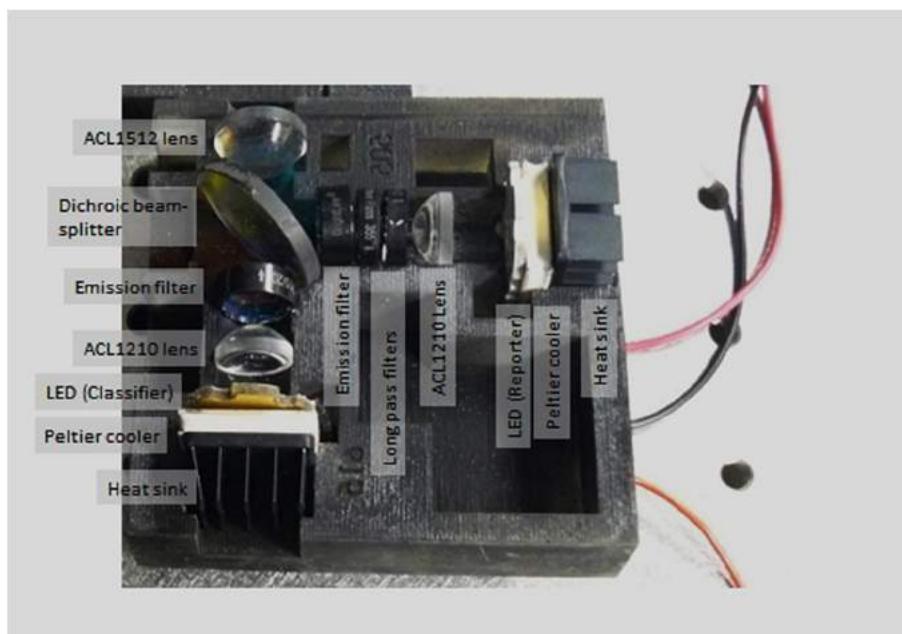
Fig. 11 A magnified view of the illumination system and its components.

were 10^{11}, $10^{10.5}$, 10^{10}, $10^{9.5}$, 10^{9}, $10^{8.5}$, 10^{8}, or 0 complementary DNA copies per 25-μl water. Singleplex samples containing one bead type and its complementary oligonucleotide were prepared in triplicate for each DNA concentration. Multiplex samples containing all three bead types and their complementary oligonucleotides were prepared in triplicate for 10^{11} DNA copies per sample.

Twenty-five microliters of DNA at each concentration were then mixed with 25 μl prepared complementary beads in the wells of a 96-well plate. Beads were prepared for miniature microscope imaging by removing debris from the bead solution by diluting 7-μl beads/sample at stock concentration in 1 ml 2× concentrated hybridization buffer (0.2 M Tris-HCl, 0.4 M NaCl, 0.16% Triton X-100). The bead solution was filtered through a 3.0-μm filter (WHA110412, Sigma Aldrich). The filter containing the beads was then washed in 25 μl 2× hybridization buffer/sample and centrifuged at 2500 relative centrifugal force to re-suspend the beads.

For experiments with data collected using the Luminex MAGPIX, DNA hybridization to MagPlex-TAG microsphere beads was performed according to the manufacturer's instructions. Briefly, beads were prepared for MAGPIX processing by diluting 2 μl beads/sample at stock concentration in 23 μl 2× hybridization buffer. Diluted beads were mixed in a 96-well plate with a dilution series of DNA target as described above.

After samples were prepared with DNA and beads in a 96 -well plate, the plate was sealed with film (MSA-5001, Biorad) and incubated in a thermal cycler. After an initial 90 s at 96°C, the plate was incubated for 30 min at 37°C. At the end of the initial incubation period, 25 μl 20 μg/ml streptavidin phycoerythrin (S866, Life Technologies) in 1 × hybridization buffer was added to each sample. The plate was incubated for an additional 15 min, removed from the thermal cycler, and placed in the Luminex MAGPIX or processed for imaging on the miniature microscope.

Samples were processed for imaging on the miniature microscope by washing twice with 1 × hybridization buffer on a magnetic stand, with the supernatant discarded after the final wash. Two point 5 μl of the washed beads were then placed on a rinsed slide in the center of a spacer (S24737, Life Technologies) and sealed with a #0 coverslip (260366, Ted Pella) and clear nail polish on the edges.

2.6 Image Acquisition

The same sample bead batch used for imaging experiments with the MAGPIX was later used for imaging experiments with the miniature microscope experiments. Samples were imaged on the MAGPIX and on the miniature microscope within 2 h of preparation. All images acquired with the miniature microscope were captured using custom software. The illumination system of the miniature microscope interfaced with an LED driver (DC4100, Thorlabs). The driver was triggered automatically through a software command to illuminate the sample. Once an LED was triggered, an image was captured and saved automatically.

Eleven images were acquired in each fluorescence channel over exposure times ranging from 10 to 1000 ms due to the large dynamic range of signal in the classifier and reporter channels. One dark frame image was also acquired at each exposure time for image correction purposes. Typical images acquired in classifier 1 and classifier 2 channels at exposure time of 300 ms are shown in Fig. 12.

2.7 Miniature Microscope Image Analysis

MATLAB version R2014a (MathWorks) was used to analyze images acquired using the miniature microscope. The flowchart of image processing operations is illustrated in Fig. 13.

The dynamic range of signals analyzed by the miniature fluorescence microscope spans 4 orders of magnitude. Due to the limited dynamic range of the detector (Chameleon USB 2.0, Point Gray, Canada), detection of the fluorescent signal is performed on high dynamic range (HDR) images, a sequence of numerically merged low dynamic range (LDR) raw images acquired at increasing exposure times (typically eleven images obtained over an evenly spaced exposure time range of 10 to 1000 ms). Each fluorescent LDR image in our system is accompanied by a dark image acquired at an identical exposure time with the light source turned off. In the first step of data processing, all LDR images and their corresponding dark images are loaded into computer memory. In the next step, dark images are subtracted from the corresponding fluorescent images. The Chameleon camera image detector is larger than the designed image circle of the miniature microscope; for this reason, processed raw fluorescent images are multiplied in the next step by a circular binary mask. The mask has a central area filled with
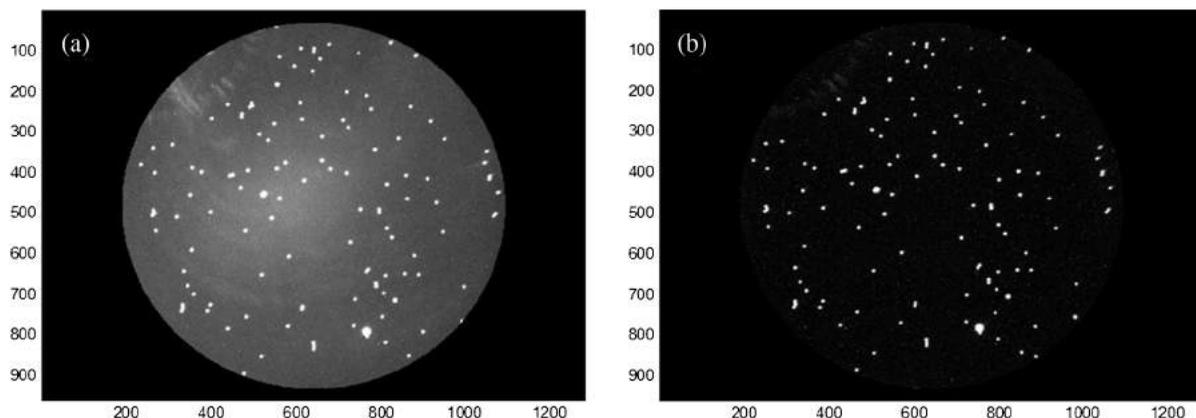
Fig. 12 Images taken with the miniature microscope from the (a) classifier 1 channel and (b) classifier 2 channel at an exposure time of 300 ms. Note that due to filter spectral characteristic, classifier 1 channel exhibits stronger background signal.
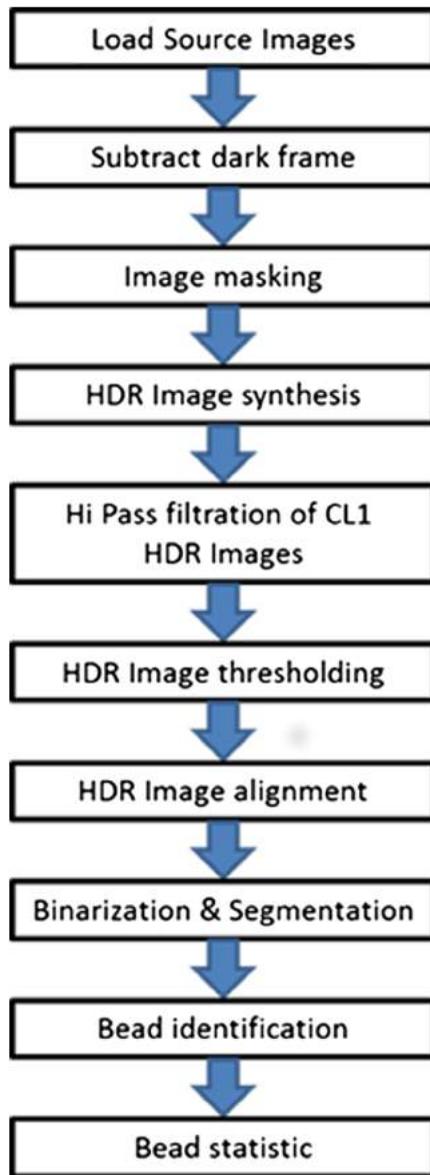
Fig. 13 Image processing algorithm and flow of operation diagram.

Fig. 14 An example of a postprocessed HDR image from the reporter channel of bead 39 tagged with 10^{11} copies of DNA (detailed description of image processing operations in the main text). Please note beads intensity variations, caused by difference in concentration of target analyte.

ones which encompasses the intended FOV of the microscope. HDR image synthesis from a series of masked LDR is performed next. The resultant HDR fluorescent images are stored in double floating point format in order to preserve the dynamic range of the signal. Due to spectral and spatial characteristics of the light source and spectral leakage of the excitation/emission filter combination, images acquired in the CL1 fluorescent channel suffer from low spatial frequency background variations. To spatially unify the intensity distribution within CL1 HDR images, we subtract the background obtained by parameterized median filtration of the source CL1 HDR image. Typically, we use a median filter with a kernel size of 41 pixels in order to obtain a smooth, slowly varying background intensity approximation. A sample filtered HDR image from the reporter channel is shown in Fig. 14.

Next, during nonlinear low pass filtration, we mask all pixels of HDR images with intensity below a preset threshold (typically 15,000 intensity counts) and leave all other pixels unchanged.
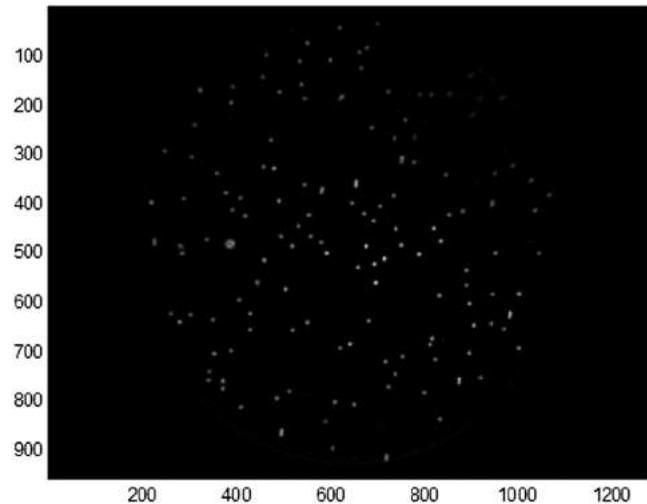
This filtering removes random noise and prepares the images for the next step of data processing, which is image alignment. We designed the optical system of the microscope using multiple monochromatic system configurations. As a result, in order to acquire sharp images in each of the mutually separated fluorescent channels, it is necessary to manually adjust the working distance of the microscope. Micromovement of the objective assembly within the system chassis is the main reason behind relative lateral shifts between HDR images. We spatially align the fluorescent HDR images using parameterized two-dimensional (2-D) correlation. During 2-D alignments, we minimize the sum of absolute difference between intensity values of overlapping pixels. Aligned fluorescent HDR images are binarized using global intensity threshold levels adjusted separately for each spectral channel. Binarized fluorescent images are segmented and basic statistic metrics of segments are calculated (area, width, height, mean intensity, median intensity, etc.). In the next step of image processing, we remove segments that do not correspond in fluorescent HDR images to isolated beads. We filter out unwanted segments using morphological criteria (pixel count, height, width, etc.) together with segment intensity conditions to select only single, isolated, nonclustered beads. Segments that correspond to same bead in filtered, binarized, and segmented images of sample, recorded through classifier 1 and 2 filters are identified next. In the final step, a scatter plot called "bead map" is created. The mean intensity of the bead in the classifier channels is used to mark a bead location in Cartesian coordinate system and the intensity of a bead in the reporter channel is used to quantify the target analyte.

2.8 Luminex MAGPIX Experiments

The Luminex MAGPIX was used according to manufacturer recommendations with the stage preheated to 37°C. Fluorescence intensity for each bead was measured and median fluorescence intensity was reported for each bead type in every sample. All data were saved and exported to Microsoft Excel for analysis.
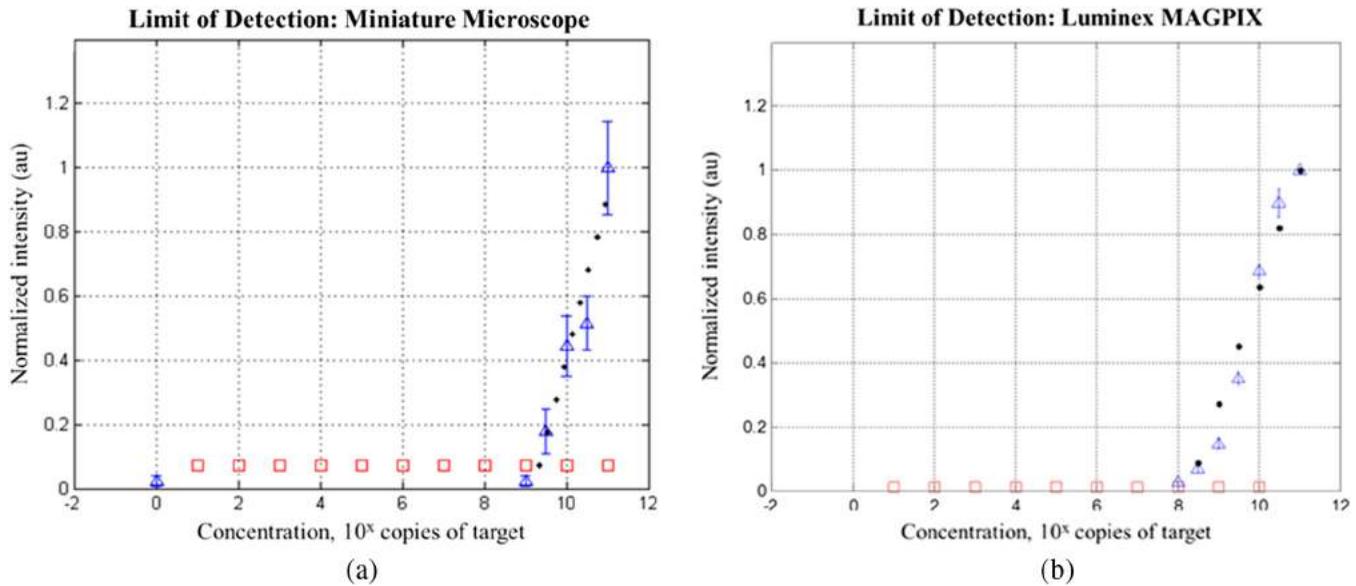
Fig. 15 The two figures above illustrate (a) limits of detection of the miniature microscope from a single-plexed experiment that used bead type #39 and (b) Luminex MAGPIX. Normalized intensity is plotted on the *y*-axis and concentration in 10^x copies of target is plotted on the *x*-axis. The limit of detection is calculated from the intersection of the baseline (red squares) with the measured median intensities at each concentration (black dots). The limit of detection of the miniature microscope was $10^{9.3}$ copies of target (synthetic DNA). For Luminex's MAGPIX, the limit of detection was found to be $10^{8.0}$ copies of target in one experiment. MAGPIX's limit of detection is reported to be between $10^{9.8}$ and $10^{10.6}$ copies of target in the literature.[16]

3 Results and Discussion

3.1 Limit of Detection: Miniature Microscope and Luminex MAGPIX

In a dilution series experiment conducted on the miniature microscope and the MAGPIX system, six bead samples were imaged with different levels of the target (copies of synthetic DNA). The target concentrations were $10^{9.0}$, $10^{9.5}$, $10^{10.0}$, $10^{10.5}$, and $10^{11.0}$ copies of synthetic DNA in addition to a nontarget control (shown as 100 copies of DNA in all subsequent figures) on the miniature microscope. MAGPIX experiments included $10^{8.0}$, $10^{8.5}$, $10^{9.0}$, $10^{9.5}$, $10^{10.0}$, $10^{10.5}$, and $10^{11.0}$ synthetic DNA copies and a nontarget control.

For the same sample bead batch, the miniature system reached a limit of detection of $10^{9.3}$ copies of target (synthetic DNA), whereas the limit of detection on the MAGPIX was found to be $10^{8.0}$ copies of target. MAGPIX's limit of detection is reported to be between $10^{9.8}$ and $10^{10.6}$ copies of target in the literature.[16] Limit of detection plots are shown in Fig. 15. The line of best fit is plotted in black dots; the normalized median intensity at each concentration is plotted in blue triangles. The red squares plotted at a concentration of zero represents the nontarget control sample, which was composed of beads with no DNA. Multiplex experiments demonstrated comparable results to singleplex samples containing the same amount of target (data not shown).

The limit of detection of the miniature microscope was found to be consistent over a series of independent experiments and ranged between $10^{9.2}$ and $10^{9.6}$. Results with Luminex's MAGPIX had a larger distribution and the limit of detection varied between $10^{8.0}$ and $10^{10.8}$. This is consistent with results reported in literature,[30] although the limit of detection may be

target-dependent. Luminex recommends using concentrations on the order of $10^{11.0}$ or above for consistent measurements.

3.2 Analyte Classification

Figure 16 shows a "bead map," which is a 2-D scatter plot of the measured intensity of beads in classifier channel 2 versus the measured intensity of beads in classifier channel 1. This bead map represents a multiplexed sample containing three different
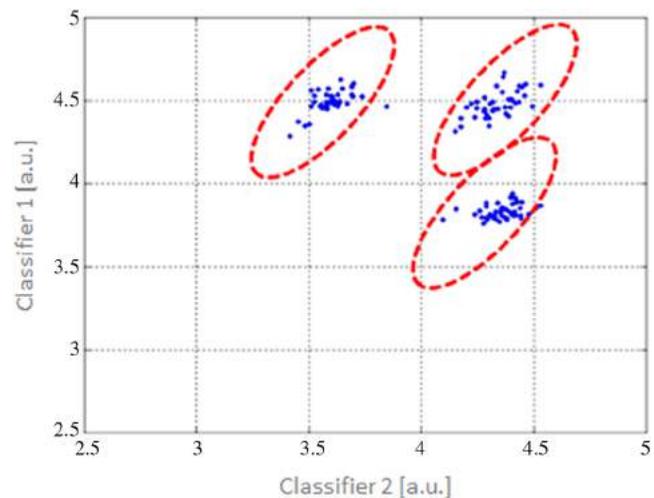
Fig. 16 A bead map from a multiplexed bead sample imaged on the miniature microscope. The sample contains 137 total beads composed of three distinct bead types, which can be resolved into three distinct groups (outlined with red ellipses). Each group is spaced ~0.6 units apart in the *y*-direction and 0.8 units apart in the *x*-direction.

bead types, imaged with the miniature microscope. Each blue dot represents the mean intensity of the brightest 25 pixels in one bead in a sample of 137 beads. The centers of each group are spaced ~0.6 units apart in the *x*-direction and ~0.8 units apart in the *y*-direction. The red dashed ellipses were arbitrarily drawn on top of the clusters to highlight the three bead groups. The separation of the tight groups of individual points illustrates the ability of our system to classify different analytes in a multiplexed sample. This method of visualizing the bead distribution also allows us to quantify the number of pathogens that can be analyzed in one sample by our device.

4 Conclusions

We developed a 3-D printed prototype of a miniature optical detection platform. Our device achieved diffraction-limited performance superior to commercially available optics at a single wavelength. For proof-of-concept applications, the miniature microscope successfully differentiated multiple bead types in a single multiplexed sample and exhibited a limit of detection comparable to a commercial bead-based assay system at $10^{9.3}$ copies of synthetic DNA. These experiments demonstrated the ability of a low-cost, rapid-prototype device with simplified, inexpensive hardware to produce a comparable limit of detection to a commercially available system.

The cost of the prototype device is estimated at 1.5 orders of magnitude less than the commercially available system. In the future, mass production of the lenses and optomechanical components via injection molding, as well as selection of specialized electronic components may reduce manufacturing costs. Additionally, mass production of filters via methods such as deposition on plastic substrates could further reduce cost, resulting in a device with a price tag suitable for POC applications in low-resource areas. Rapid prototyping techniques, which we validated for possible POC use in this preliminary application, will allow relatively rapid development of future generations of miniature POC optical readout devices for different biological applications, such as infectious disease detection or complete blood counts.

Acknowledgments

References

1. General Assembly of the United Nations, *High-Level Meeting on AIDS; United Nations*, New York (2006).
2. R. W. Peeling, P. G. Smith, and P. M. M. Bossuyt, "A guide for diagnostic evaluations," *Nat. Rev. Microbiol.* **9**(9), S2–S6 (2010).
3. M. C. Pierce et al., "Optical systems for point-of-care diagnostic instrumentation: analysis of imaging performance and cost," *Ann. Biomed. Eng.* **42**(1), 231–240 (2014).
4. D. N. Breslaur et al., "Mobile phone based clinical microscopy for global health applications," *PLoS One* **4**, e6320 (2009).
5. D. Fletcher et al., "Cellscope," http://cellscope.com (21 April 2015).
6. A. Skandarajah et al., "Quantitative imaging with a mobile phone microscope," *PLoS One* **9**(5), e96906 (2014).
7. H. Zhu et al., "Optofluidic fluorescent imaging cytometry on a cell phone," *Anal Chem.* **83**(17), 6641–6647 (2011).
8. A. R. Miller et al., "Portable, battery-operated, low-cost, bright field and fluorescence microscope," *PLoS One* **5**, e11890 (2010).
9. K. R. Steingard et al., "Sputum processing methods to improve the sensitivity of smear microscopy for tuberculosis: a systematic review," *Lancet Infect. Dis.* **6**(10), 664–674 (2006).
10. D. Jones et al., "McArthur revisited: fluorescence microscopes for field diagnostics," *Trends Parasitol.* **23**(10), 468–469 (2007).
11. J. S. Kim et al., "Multiplexed detection of bacteria and toxins using a microflow cytometer," *Anal. Chem.* **81**(13), 5426–5432 (2009).
12. J. Vrbarg et al., "Catch and release: integrated system for multiplexed detection of bacteria," *Anal. Chem.* **85**(10), 4944–4950 (2013).
13. D. A. Vignali, "Multiplexed particle-based flow cytometric assays," *J. Immunol. Methods* **243**(1–2), 243–255 (2000).
14. IDEXX, "ELISA technical guide," http://www.idexx.com/pubweb-resources/pdf/en_us/livestock-poultry/elisa-technical-guide.pdf (2015).
15. S. X. Leng et al., "ELISA and multiplex technologies for cytokine measurement in inflammation and aging research," *J. Gerontol.* **63**, 879–884 (2007).
16. T. Watterson and S. Wallace, *Multiplexed ELISA Validation*, Quansys Biosciences, 2013, http://www.quansysbio.com/new/wp-content/uploads/2013/12/Multiplex-ELISA-Validation_11-2013.pdf (10 April 2014).
17. *Instruments*, Meso Scale Diagnostics LLC, 2014, http://www.mesoscale.com/products_and_services/instrumentation/ (16 April 2014).
18. Luminex Corp., "Overcoming the cost and performance limitations of ELISA with xMAP® Technology:xMAP technical note [white paper]," 2010, http://www.bio-rad.com/webroot/web/pdf/lsr/literature/6313.pdf (10 April 2014).
19. V. Gubala et al., "Point of care diagnostics: status and future," *Anal. Chem.* **84**(2), 487–515 (2012).
20. R&D Systems, "Tools for cell biology research. Luminex screening & performance assays bead-based multiplex kits," 2013, http://www.rndsystems.com/resources/images/27612.pdf (10 April 2014).
21. Luminex Corp., "MAGPIX: Multiply the Power of Your Potential [sell sheet]," 2011, https://www.luminexcorp.com/clinical/instruments/magpix/ (10 April 2014).
22. S. M. Landau et al., "Design and evaluation of an ultra-slim objective for in-vivo deep optical biopsy," *Opt. Express* **18**(5), 4758–4775 (2010).
23. J. M. Cavagnaro, "Polymer optics: progress in plastic optics follows advances in materials and manufacturing," 2011, http://www.laser-focusworld.com/articles/print/volume-47/issue-9/features/polymer-optics-progress-in-plastic-optics-follows-advances-in-materials-and-manufacturing.html (19 February 2014).
24. M. K. Kyrish et al., "Ultra-slim plastic endomicroscope objective for non-linear microscopy," *Opt. Express* **19**(8), 7603–7615 (2011).
25. S. Baumer, *Handbook of Plastic Optics*, 2nd ed., Wiley-VCH, Verlag GmbH and Co. KGaA, Weinheim (2011).
26. M. Kyrish and T. S. Tkaczyk, "Achromatized endomicroscope for optical biopsy," *Biomed. Opt. Express* **2**(2), 287–297 (2013).
27. A. Kobayashi and K. Hirakawa, "Ultraprecision machining of plastics. Part 1: Polymethyl methacrylate," *Polym-Plast. Technol. Eng.* **22**(1), 15–25 (1984).
28. J. W. Carr and C. Feger, "Ultraprecision machining of polymers," *Precis. Eng.* **15**(4), 221–237 (1993).
29. A. V. Arecchi, T. Messadi, and R. J. Koshel, *Field Guide to Illumination*, SPIE Press, Bellingham, Washington (2007).
30. "MAGPLEX®-TAG™ microspheres comparative data white paper," Luminex, 2011, http://www.luminexcorp.com/prod/groups/public/documents/lmnxcorp/adv-003-magplex-tag-comparativ.pdf (2 October 2014).

Alessandra Forcucci studied biomedical engineering at Boston University. She is currently a PhD candidate at Rice University in the Department of Bioengineering. Her thesis research is focused on the development of low-cost, high-performance optical instrumentation for detecting and diagnosing infectious disease at the point of care in low-resource settings.

Michal Emanuel Pawlowski received his MSc Eng. in applied optics from the Warsaw University of Technology in 1997 and received PhD from the same university in 2002. He was a postdoctoral student at the University of Electro-Communications in Tokyo between 2003 and 2005. Currently, he works at Rice University as a research scientist, where his main interests are applied optics, optical design, and bioengineering.

Zachary Crannell studied bioengineering at Texas A&M University, then worked in industry for 4 years before completing his PhD at Rice University. His thesis research was focused on developing low-cost

molecular assays for diagnosing infectious diseases in low-resource settings.

Ina Pavlova is a research scientist at Columbia University Medical Center, applying her background in deep tissue microscopy to study mechanisms of memory formation. Her research focuses on applying optical spectroscopy and imaging to solve problems in biomedical research and medicine. Previously, she was involved in the development of low-cost, imaging devices for the readout of bioassays. Her doctoral and postdoctoral research focused on optical imaging for the minimally invasive detection of cancer.

Rebecca Richards-Kortum is the Malcolm Gillis University professor at Rice University. Her research focuses on the development of

point-of-care and pediatric technologies to improve healthcare in low-resource settings.

Tomasz S. Tkaczyk has been an associate professor of bioengineering and electrical and computer engineering at Rice University since 2007, where he develops modern optical instrumentation biomedical applications. He received his MS and PhD degrees from the Institute of Micromechanics and Photonics, Department of Mechatronics, Warsaw University of Technology. In 2003, after his postdoctoral training, he worked as a research professor at the College of Optical Sciences, University of Arizona. His research interests include endoscopy, cost-effective high-performance optics for diagnostics, and multidimensional snapshot imaging systems.